

Trajectory-Switching Algorithm for a MEMS Gyroscope

Sungsu Park, Roberto Horowitz, *Member, IEEE*, Sung Kyung Hong, and Yoonsu Nam

Abstract—The motion of a conventional force-balancing-controlled gyroscope in a mode-matched operation does not have sufficient persistence of excitation, and as a result, all major fabrication imperfections cannot be identified and compensated for. This paper presents an adaptive force-balancing control for a microelectromechanical-system z -axis gyroscope using a trajectory-switching algorithm. The proposed adaptive force-balancing control supplies additional richness of excitation to the internal dynamics of the gyroscope by switching the trajectory of the proof mass of the gyroscope, and it provides quadrature compensation, drive- and sense-axis frequency tuning, and closed-loop identification of the angular rate without the measurement of input/output phase difference. This algorithm also identifies and compensates the cross-damping terms which cause zero-rate output.

Index Terms—Adaptive control, force-balancing control, gyroscope, microelectromechanical systems (MEMS), trajectory switching.

I. INTRODUCTION

MOST microelectromechanical-system (MEMS) gyroscopes are vibratory rate gyroscopes that have structures fabricated on polysilicon or crystal silicon, and the mechanical main component is a two degree-of-freedom vibrating structure, which is capable of oscillating on two directions in a plane. Their operating physics is based on the Coriolis effect. When the gyroscope is subjected to an angular velocity, the Coriolis effect transfers energy from one vibrating mode to another. The response of the second vibrating mode provides information about the applied angular velocity. Ideally, in the conventional mode of operation, the vibrating modes of a MEMS gyroscope are supposed to remain mechanically uncoupled, their natural frequencies should be matched, and the gyroscope's output should only be sensitive to angular velocity. In practice, however, fabrication imperfections and environmental variations are always present, resulting in a frequency of oscillation mismatch between the two vibrating modes and a coupling between the two mechanical vibration modes through off-diagonal

Manuscript received March 10, 2006; revised August 8, 2007.

S. Park and S. K. Hong are with the Department of Aerospace Engineering, Sejong University, Seoul 143-747, Korea (e-mail: sungsu@sejong.ac.kr; skhong@sejong.ac.kr).

R. Horowitz is with the Department of Mechanical Engineering, University of California at Berkeley, Berkeley, CA 94720 USA (e-mail: horowitz@me.berkeley.edu).

Y. Nam is with the Department of Mechanical and Mechatronics Engineering, Kangwon National University, Chuncheon 200-701, Korea (e-mail: nys@kangwon.ac.kr).

Color versions of one or more of the figures in this paper are available online at <http://ieeexplore.ieee.org>.

Digital Object Identifier 10.1109/TIM.2007.908597

terms in the stiffness and damping matrices. These imperfections degrade the gyroscope's performance and cause a false output [1], [2].

Currently, force-balancing feedback control schemes [3]–[5] have widely been used to cancel the effect of the off-diagonal terms in the stiffness matrix, which is referred to as the quadrature error, as well as to increase the bandwidth and dynamic range of the gyroscope beyond the open-loop mode of operation. However, they rely on the exact measurement of the input/output phase difference, and moreover, they are inherently sensitive to some types of fabrication imperfections which can be modeled as cross-damping terms, which produce zero-rate output (ZRO).

In this paper, we develop an adaptive force-balancing control scheme for a MEMS z -axis gyroscope using a trajectory-switching algorithm. This adaptive algorithm provides quadrature compensation, drive- and sense-axis frequency tuning, and closed-loop identification of the angular rate without the measurement of the input/output phase difference. This algorithm also identifies and compensates the cross-damping terms and does not produce ZRO.

In the next section, the dynamics of MEMS gyroscopes are developed and analyzed by accounting for the effect of the fabrication imperfections. The conventional force-balancing control is reviewed and reinterpreted for the extension to an adaptive scheme in Section III. In Section IV, a trajectory-switching strategy is proposed to supply additional richness of excitation to the internal dynamics of the gyroscope. In Section V, an adaptive control is developed based on the trajectory-switching algorithm. Finally, computer simulations are performed in Section VI.

II. DYNAMICS OF MEMS GYROSCOPES

Common MEMS vibratory-gyroscope configurations include a proof mass suspended by spring suspensions, electrostatic actuation, and sensing mechanisms for forcing an oscillatory motion and sensing of the position and velocity of the proof mass. These mechanical components can be modeled as mass, spring, and damper system. Fig. 1 shows a simplified model of a MEMS gyroscope having two degrees of freedom in the associated Cartesian reference frames.

By assuming that the motion of the proof mass is constrained to be only along the x – y plane by making the spring stiffness in the z -direction much larger than in the x - and y -directions, the measured angular rate is almost constant over a long enough time interval, and linear accelerations are canceled out, either as an offset from the output response or by applying

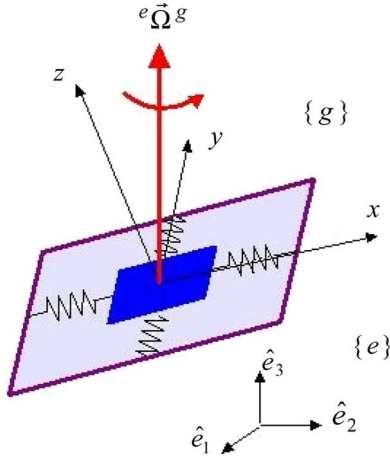


Fig. 1. Model of a MEMS z -axis gyroscope.

countercontrol forces, and then, the equation of motion of a gyroscope is simplified as follows:

$$\begin{aligned} m\ddot{x} + d_1\dot{x} + (k_1 - m(\Omega_y^2 + \Omega_z^2))x + m\Omega_x\Omega_y y &= \tau_x + 2m\Omega_z\dot{y} \\ m\ddot{y} + d_2\dot{y} + (k_2 - m(\Omega_x^2 + \Omega_z^2))y + m\Omega_x\Omega_y x &= \tau_y - 2m\Omega_z\dot{x} \end{aligned} \quad (1)$$

where x and y are the coordinates of the proof mass relative to the gyroframe, $d_{1,2}$ and $k_{1,2}$ are the damping and spring coefficients, $\Omega_{x,y,z}$ denotes the angular-velocity components along each axis of the gyroframe, and $\tau_{x,y}$ denotes the control forces. The two last terms in (1), which are $2m\Omega_z\dot{x}$ and $2m\Omega_z\dot{y}$, are due to the Coriolis forces and are the terms that are used to measure the angular rate Ω_z .

As shown in (1), in an ideal gyroscope, only the component of the angular rate along the z -axis Ω_z causes a dynamic coupling between the x - and y -axes under the assumption that $\Omega_{x,y}^2 \approx \Omega_x\Omega_y \approx 0$. In practice, however, small fabrication imperfections always occur, which cause dynamic coupling between the x - and y -axes through the asymmetric spring and damping terms. By taking into account the fabrication imperfections, the dynamic equations (1) are modified as follows [6]:

$$\begin{aligned} m\ddot{x} + d_{xx}\dot{x} + d_{xy}\dot{y} + k_{xx}x + k_{xy}y &= \tau_x + 2m\Omega_z\dot{y} \\ m\ddot{y} + d_{xy}\dot{x} + d_{yy}\dot{y} + k_{xy}x + k_{yy}y &= \tau_y - 2m\Omega_z\dot{x}. \end{aligned} \quad (2)$$

Equation (2) is the governing equation for a MEMS z -axis gyroscope. The fabrication imperfections mainly contribute to the asymmetric spring and damping terms k_{xy} and d_{xy} . Therefore, these terms are unknown but can be assumed to be small. The x - and y -axis spring and damping terms are mostly known but have unknown variations from their nominal values. The proof mass can very accurately be determined. The components of angular rate along the x - and y -axes are absorbed as part of the spring terms as unknown variations. Note that the spring coefficients k_{xx} and k_{yy} also include the electrostatic spring softness.

Based on m , q_0 , and ω_0 , which are the reference mass (i.e., a proof mass of the gyroscope), the length, and the natural

resonance frequency, respectively, the nondimensionalization of (2) can be done as follows:

$$\begin{aligned} \ddot{x} + \frac{\omega_x}{Q_x}\dot{x} + d_{xy}\dot{y} + \omega_x^2 x + \omega_{xy}y &= \tau_x + 2\Omega_z\dot{y} \\ \ddot{y} + d_{xy}\dot{x} + \frac{\omega_y}{Q_y}\dot{y} + \omega_{xy}x + \omega_y^2 y &= \tau_y - 2\Omega_z\dot{x} \end{aligned} \quad (3)$$

where Q_x and Q_y are the x - and y -axis quality factors, respectively, $\omega_x = \sqrt{k_{xx}/(m\omega_0^2)}$, $\omega_y = \sqrt{k_{yy}/(m\omega_0^2)}$, $\omega_{xy} = k_{xy}/(m\omega_0^2)$, $d_{xy} \leftarrow d_{xy}/(m\omega_0)$, $\Omega_z \leftarrow \Omega_z/\omega_0$, $\tau_x \leftarrow \tau_x/(m\omega_0^2 q_0)$, and $\tau_y \leftarrow \tau_y/(m\omega_0^2 q_0)$.

III. MOTIVATION

The general tasks of the conventional drive-axis feedback control in a vibratory gyroscope can be reinterpreted as keeping the total energy level of the device constant while forcing the trajectory of the proof mass of the gyroscope to be a straight line in the x - y plane when no angular rate is present. The force-balancing control can also be interpreted as the task of maintaining a straight-line motion, even under the presence of the angular rate. In order to understand how the angular rate can be measured by maintaining a gyroscope straight-line motion, we will first study the dynamic response of an ideal planar vibratory gyroscope. This ideal gyroscope under the presence of the angular rate is defined as follows:

$$\ddot{q} + \omega_0^2 q = -2\Omega\dot{q} \quad (4)$$

where $q = [x \ y]^T$, and $\Omega = \begin{bmatrix} 0 & -\Omega_z \\ \Omega_z & 0 \end{bmatrix}$. Equation (4) presents a two degree-of-freedom pure spring-mass system with the same natural frequency ω_0 in both axes, which is oscillating on a rotating frame with an angular rate Ω_z . When no angular rate is present, depending on whether the initial displacement vector is parallel to the velocity vector or not, this ideal gyroscope will either oscillate along the straight line or along an ellipsoid trajectory. When the gyroscope is rotating, the line of oscillation precesses because the Coriolis acceleration causes a transfer of energy between the two axes of the gyroscope while conserving the total energy of the gyroscope. This can be shown by defining the total energy E and the angular momentum P of the gyroscope, respectively, as

$$\begin{aligned} E &= \frac{1}{2} (\dot{q}^T \dot{q} + \omega_0^2 q^T q) \\ P &= q^T S \dot{q} = q_S^T \dot{q} \end{aligned} \quad (5)$$

where $S = \begin{bmatrix} 0 & 1 \\ -1 & 0 \end{bmatrix}$, and $q_S = S^T q$.

Note that the angular momentum is a good measure of how much the motion of a gyroscope deviates from a straight-line oscillation since in a straight-line oscillation, $P = 0$ [6]. The time derivatives of the total energy and the angular momentum are

$$\begin{aligned} \dot{E} &= \dot{q}^T \ddot{q} + \omega_0^2 \dot{q}^T q = \dot{q}^T (-\omega_0^2 q - 2\Omega\dot{q}) + \omega_0^2 \dot{q}^T q = 0 \\ \dot{P} &= \dot{q}^T S \dot{q} + q^T \ddot{q} = q_S^T (-\omega_0^2 q - 2\Omega\dot{q}) = -2\Omega_z q^T \dot{q}. \end{aligned} \quad (6)$$

From (6), it is clear that the Coriolis-acceleration term does not change the total energy and only causes precession, i.e., a change of angular momentum. When no angular rate is present, the angular momentum is also conserved. For example, if the initial angular momentum is zero or, equivalently, the displacement and velocity vectors are parallel, the oscillation will remain in a straight line. Therefore, this suggests that we may be able to measure the angular rate by generating a control action such that the angular momentum is not changed, even under the presence of the angular rate. Unfortunately, in the case of nonideal gyroscopes, because of damping terms, the total energy is not conserved. Moreover, because of quadrature errors and damping terms, the angular momentum is not conserved even when the angular rate is zero. Therefore, one possible approach to measure the angular rate with a nonideal gyroscope is to generate control forces such that a gyroscope emulates the behavior of an ideal gyroscope operating under no angular rate or, equivalently, such that the total energy is kept unchanged and the angular momentum converges to zero (i.e., the trajectory converges to a straight-line oscillation).

IV. TRAJECTORY-SWITCHING STRATEGY

In this section, we will formulate a control law and parameter adaptation algorithms for the z -axis gyroscope such that the total energy error and the angular momentum asymptotically converge to zero. The total energy error is defined by

$$\tilde{E} = \frac{1}{2} (\dot{q}^T \dot{q} + \omega_0^2 q^T q) - E_0 \quad (7)$$

where E_0 is a prescribed intended energy level. Note that the total energy is computed based on the ideal gyroscope parameters. Now, let us rewrite the nondimensional gyroscope equation (3) as follows:

$$\ddot{q} + D\dot{q} + Kq = \tau - 2\Omega\dot{q} \quad (8)$$

where $K = \begin{bmatrix} \omega_x^2 & \omega_{xy} \\ \omega_{xy} & \omega_y^2 \end{bmatrix}$, $D = \begin{bmatrix} \omega_x/Q_x & d_{xy} \\ d_{xy} & \omega_y/Q_y \end{bmatrix}$, and these are assumed to be constant. Consider the following positive definite function (PDF):

$$V = \frac{1}{2} (\gamma_E \tilde{E}^2 + \gamma_P P^2 + \text{tr} \{ \gamma_R^{-1} \tilde{R} \tilde{R}^T + \gamma_D^{-1} \tilde{D} \tilde{D}^T + \gamma_\Omega^{-1} \tilde{\Omega} \tilde{\Omega}^T \}) \quad (9)$$

where $\gamma_{(\cdot)}$ denotes the positive constants, and

$$\tilde{R} = \hat{R} - K + \omega_0^2 I, \quad \tilde{D} = \hat{D} - D, \quad \tilde{\Omega} = \hat{\Omega} - \Omega$$

where \hat{R} , \hat{D} , and $\hat{\Omega}$ are the estimates of $R = K - \omega_0^2 I$, D , and Ω , respectively, I is an identity matrix, and $\text{tr}(M)$ defines the trace of the matrix M . The derivative of the PDF V along the trajectory of (8) is

$$\dot{V} = \gamma_E \tilde{E} \dot{\tilde{E}} + \gamma_P P \dot{P} + \text{tr} \left(\gamma_R^{-1} \tilde{R} \dot{\tilde{R}}^T + \gamma_D^{-1} \tilde{D} \dot{\tilde{D}}^T + \gamma_\Omega^{-1} \tilde{\Omega} \dot{\tilde{\Omega}}^T \right). \quad (10)$$

If the control law τ is chosen to be

$$\tau = \tau_0 + \hat{R}q + \hat{D}\dot{q} + 2\hat{\Omega}\dot{q} \quad (11)$$

where τ_0 is an auxiliary control action, which will subsequently be defined, the derivatives of the total energy error and the angular momentum can then be computed as follows:

$$\begin{aligned} \dot{\tilde{E}} &= \dot{E} = \dot{q}^T (\tau_0 + \hat{R}q + \hat{D}\dot{q} + 2\hat{\Omega}\dot{q}) \\ \dot{P} &= \dot{q}_S^T (\tau_0 + \hat{R}q + \hat{D}\dot{q} + 2\hat{\Omega}\dot{q}). \end{aligned} \quad (12)$$

Substituting (12) into (10) results in

$$\begin{aligned} \dot{V} &= (\gamma_E \tilde{E} \dot{q} + \gamma_P P q_S)^T \tau_0 \\ &+ (\gamma_E \tilde{E} \dot{q} + \gamma_P P q_S)^T (\hat{R}q + \hat{D}\dot{q} + 2\hat{\Omega}\dot{q}) \\ &+ \text{tr} \left(\gamma_R^{-1} \tilde{R} \dot{\tilde{R}}^T + \gamma_D^{-1} \tilde{D} \dot{\tilde{D}}^T + \gamma_\Omega^{-1} \tilde{\Omega} \dot{\tilde{\Omega}}^T \right). \end{aligned} \quad (13)$$

If τ_0 is chosen to be

$$\tau_0 = -(\gamma_E \tilde{E} \dot{q} + \gamma_P P q_S) \quad (14)$$

then (13) becomes

$$\begin{aligned} \dot{V} &= -(\gamma_E \tilde{E} \dot{q} + \gamma_P P q_S)^T (\gamma_E \tilde{E} \dot{q} + \gamma_P P q_S)^T \\ &+ \text{tr} \left\{ \tilde{R} \left(\gamma_R^{-1} \dot{\tilde{R}}^T - \frac{1}{2} \dot{q} \tau_0^T - \frac{1}{2} \tau_0 \dot{q}^T \right) \right. \\ &+ \tilde{D} \left(\gamma_D^{-1} \dot{\tilde{D}}^T - \frac{1}{2} \dot{q} \tau_0^T - \frac{1}{2} \tau_0 \dot{q}^T \right) \\ &\left. + \tilde{\Omega} \left(\gamma_\Omega^{-1} \dot{\tilde{\Omega}}^T - \dot{q} \tau_0^T + \tau_0 \dot{q}^T \right) \right\}. \end{aligned} \quad (15)$$

Equation (15) suggests the following adaptation laws for the estimates \hat{R} , \hat{D} , and $\hat{\Omega}$:

$$\begin{aligned} \dot{\hat{R}} &= \frac{1}{2} \gamma_R (\tau_0 q^T + q \tau_0^T) \\ \dot{\hat{D}} &= \frac{1}{2} \gamma_D (\tau_0 \dot{q}^T + \dot{q} \tau_0^T) \\ \dot{\hat{\Omega}} &= \gamma_\Omega (\tau_0 \dot{q}^T - \dot{q} \tau_0^T) \end{aligned} \quad (16)$$

in order to guarantee that \dot{V} will be negative semidefinite

$$\dot{V} = -[\tilde{E} \quad P] \begin{bmatrix} \gamma_E^2 \dot{q}^T \dot{q} & \gamma_E \gamma_P \dot{q}^T q_S \\ \gamma_E \gamma_P \dot{q}^T q_S & \gamma_P^2 q^T q \end{bmatrix} \begin{bmatrix} \tilde{E} \\ P \end{bmatrix} \leq 0. \quad (17)$$

From (17), it is easy to show the convergence of \tilde{E} and P to zero by using Barbalat's lemma [7]. However, this by itself does not guarantee the convergence of parameter errors \tilde{R} , \tilde{D} , and $\tilde{\Omega}$ to zero. Since the main role of a gyroscope is to measure the applied angular rate, which, in this context, requires that $\tilde{\Omega} = 0$, we need to determine the conditions that guarantee the asymptotic convergence of $\tilde{\Omega}$ to zero. Regarding this, we have the following results.

Theorem 1: With the control laws (11) and (14) and the adaptation algorithm (16), the following results hold for the system (8).

- 1) The convergence of the angular-rate estimate $\hat{\Omega}_z$ to its true value is guaranteed only when the damping matrix D is known.
- 2) The angular-rate estimate error $\tilde{\Omega}_z$ is biased by one half of the off-diagonal damping term d_{xy} if the trajectory is forced to converge to a straight-line oscillation along the x -axis and if no adaptive compensation is utilized on the off-diagonal damping terms.

Proof: By using Barbalat’s lemma, one can easily show that, as time $t \rightarrow \infty$

$$\dot{E} = \dot{q}^T (\tilde{R}q + \tilde{D}\dot{q} + 2\tilde{\Omega}\dot{q}) \rightarrow 0 \tag{18}$$

$$\dot{P} = q_S^T (\tilde{R}q + \tilde{D}\dot{q} + 2\tilde{\Omega}\dot{q}) \rightarrow 0 \tag{19}$$

$$P = q_S^T \dot{q} \rightarrow 0. \tag{20}$$

Convergence property (20) implies that the trajectory of the system converges to a straight-line oscillation in the x - y plane. By (20), (18) and (19) imply that

$$(\tilde{R}q + \tilde{D}\dot{q} + 2\tilde{\Omega}\dot{q}) \rightarrow 0 \tag{21}$$

since \dot{q} and q_S^T converge to be perpendicular to each other. The convergence behavior of (21) at the instance of $q = 0$ and $\dot{q} = 0$ shows that each term of (21) should independently converge to zero, i.e.,

$$\tilde{R}q \rightarrow 0 \quad \text{and} \quad (\tilde{D} + 2\tilde{\Omega})\dot{q} \rightarrow 0. \tag{22}$$

Therefore, if D is known or, equivalently, $\tilde{D} = 0$, the convergence of the angular-rate estimate to its true value can be proved since

$$2\tilde{\Omega}\dot{q} \rightarrow 0 \rightarrow \tilde{\Omega}_z \rightarrow 0 \quad \text{since} \quad \tilde{\Omega} = \begin{bmatrix} 0 & -\tilde{\Omega}_z \\ \tilde{\Omega}_z & 0 \end{bmatrix}.$$

Because the trajectory converges to a straight line, i.e., q becomes parallel to \dot{q} , (22) can be rewritten as

$$\begin{aligned} \eta(t)\tilde{R}\hat{v} &\rightarrow 0 \\ \kappa(t)(\tilde{D} + 2\tilde{\Omega})\hat{v} &\rightarrow 0 \end{aligned} \tag{23}$$

where \hat{v} is the unit vector in the x - y plane along the straight-line oscillation, and $q \rightarrow \eta(t)\hat{v}$ and $\dot{q} \rightarrow \kappa(t)\hat{v}$, where $\eta(t)$ and $\kappa(t)$ are the scalar periodic functions. This is equivalent to

$$\begin{aligned} \begin{bmatrix} \tilde{\omega}_x^2 & \tilde{\omega}_{xy} \\ \tilde{\omega}_{xy} & \tilde{\omega}_y^2 \end{bmatrix} \begin{bmatrix} \nu_x \\ \nu_y \end{bmatrix} &\rightarrow 0 \\ \begin{bmatrix} \tilde{d}_{xx} & \tilde{d}_{xy} - 2\tilde{\Omega}_z \\ \tilde{d}_{xy} + 2\tilde{\Omega}_z & \tilde{d}_{yy} \end{bmatrix} \begin{bmatrix} \nu_x \\ \nu_y \end{bmatrix} &\rightarrow 0. \end{aligned} \tag{24}$$

If the trajectory converges to be along the x -axis, i.e., $\nu_x = 1$ and $\nu_y = 0$, then

$$\tilde{\omega}_x^2 \rightarrow 0, \quad \tilde{\omega}_{xy} \rightarrow 0, \quad \tilde{d}_{xx} \rightarrow 0, \quad \text{and} \quad \tilde{\Omega}_z \rightarrow -\frac{1}{2}\tilde{d}_{xy}. \tag{25}$$

Therefore, if the trajectory is forced to converge to an oscillatory motion along the x -axis, the angular-rate estimate is biased by one half of the off-diagonal term of the damping matrix when no adaptation action is done on d_{xy} , i.e., $\tilde{\Omega}_z \rightarrow -(1/2)d_{xy}$. ■

Consequently, based on Theorem 1, the following lemma holds.

Lemma 1: If the total energy level is kept constant and the trajectory of the proof mass of a nonideal gyroscope is forced to be aligned along the drive axis, then the drive-axis frequency, the drive-axis damping, and the quadrature error can be identified and compensated for. Moreover, the applied angular rate can be estimated to the accuracy of the magnitude of the off-diagonal damping term.

In this control, the quadrature compensation does not rely on the measurement of the input/output phase difference, whereas it does in the conventional force-balancing control. However, there remains a deterministic bias in the angular-rate estimate, as in the case of the conventional force-balancing control. In a similar fashion to the conventional mode of operation, this bias term can be calibrated out. The reason why the parameters do not converge to their true values is lack of persistent excitation because of the simple internal dynamics of the gyroscope. Theorem 1 provides a hint for seeking another control strategy for guaranteeing $\tilde{\Omega}_z \rightarrow 0$. This can be achieved by supplying additional richness of excitation to the internal dynamics of the gyroscope. This is summarized in the following theorem.

Theorem 2: If the control law and the parameter adaptation algorithms are formulated such that the total energy level is kept constant and the trajectory of the proof mass converges to a straight line in one direction (\hat{v}_2), after it has first converged to a straight line in another direction (\hat{v}_1) in the x - y plane, while preserving the following conditions on parameter adaptation laws

$$\dot{R}\hat{v}_1 \rightarrow 0 \quad \text{and} \quad (\tilde{D} + 2\tilde{\Omega})\hat{v}_1 \rightarrow 0 \tag{26}$$

then all gyroscope parameter estimates, including the angular-rate estimate, converge to their true values.

Proof: By Theorem 1, the convergence properties given by (22) are achieved on \hat{v}_1 , i.e.,

$$\tilde{R}\hat{v}_1 \rightarrow 0 \quad \text{and} \quad (\tilde{D} + 2\tilde{\Omega})\hat{v}_1 \rightarrow 0. \tag{27}$$

With the condition (26), if a similar convergence is achieved along \hat{v}_2 , i.e.,

$$\tilde{R}\hat{v}_2 \rightarrow 0 \quad \text{and} \quad (\tilde{D} + 2\tilde{\Omega})\hat{v}_2 \rightarrow 0 \tag{28}$$

then (27) and (28) lead to

$$\tilde{R} \rightarrow 0 \quad \text{and} \quad (\tilde{D} + 2\tilde{\Omega}) \rightarrow 0.$$

Since \tilde{D} is a symmetric matrix and $\tilde{\Omega}$ is a skew-symmetric matrix, this implies that

$$\tilde{R} \rightarrow 0, \quad \tilde{D} \rightarrow 0, \quad \text{and} \quad \tilde{\Omega} \rightarrow 0. \quad \blacksquare$$

The next section proposes a control strategy which switches between two straight-line oscillation modes and achieves all conditions in Theorem 2.

V. TRAJECTORY FOLLOWING AND SWITCHING CONTROL

As mentioned in Theorem 2, unbiased estimation of the angular rate can be achieved if the asymptotic trajectory of the gyroscope is switched between two oscillatory motions along nonparallel vectors in the x - y plane. However, because the adaptive algorithm in Section IV deals with only the total energy and the angular momentum, it cannot control the direction of the straight-line oscillation to which the gyroscope converges. Instead of controlling the total energy and the angular momentum, one may try to control the energy level of each axis together with the angular momentum of the gyroscope. However, this is also difficult because of lack of sufficient control degrees of freedom. In this section, an alternative model reference-trajectory-following method is proposed to achieve trajectory switching. The reference trajectory is generated by an ideal gyroscope such that its total energy level is conserved, and its angular momentum is kept to zero. Therefore, the reference-trajectory-following method indirectly realizes both the goal of adaptive control in Section IV and trajectory switching.

A. Design of Adaptive Control Law

Suppose that the reference trajectory satisfies the equation of the ideal gyroscope and makes the angular momentum be zero, i.e.,

$$\begin{aligned} \ddot{q}_m + \omega_0^2 q_m &= 0 \\ P = q_m^T S \dot{q}_m &= 0 \end{aligned} \quad (29)$$

where $q_m = [x_m \ y_m]^T$. This may be realized by the following trajectory model:

$$q_m = \begin{bmatrix} \cos \alpha X_0 \sin(\omega_0 t) \\ \sin \alpha X_0 \sin(\omega_0 t) \end{bmatrix} \quad (30)$$

where α is the slope angle of the straight-line trajectory as measured from the x -axis in the x - y plane, and X_0 is the amplitude of oscillation. Similar to the adaptive control strategy based on energy and angular momentum in the previous section, the control law τ in this case is chosen to be

$$\tau = \tau_1 + \hat{R}\dot{q} + \hat{D}\dot{q} + 2\hat{\Omega}\dot{q} \quad (31)$$

where τ_1 will subsequently be defined. By defining the trajectory error as $e_p = q - q_m$, the trajectory error dynamics becomes

$$\ddot{e}_p + \omega_0^2 e_p = \tau_1 + \tilde{u} \quad (32)$$

where

$$\tilde{u} = \tilde{R}\dot{q} + \tilde{D}\dot{q} + 2\tilde{\Omega}\dot{q}.$$

Consider the following PDF candidate:

$$V = \frac{1}{2} \left(\gamma_e \dot{e}_p^T \dot{e}_p + \gamma_e \omega_0^2 e_p^T e_p + \text{tr} \left\{ \gamma_R^{-1} \tilde{R} \tilde{R}^T + \gamma_D^{-1} \tilde{D} \tilde{D}^T + \gamma_\Omega^{-1} \tilde{\Omega} \tilde{\Omega}^T \right\} \right) \quad (33)$$

where $\gamma(\cdot)$ denotes the positive constants. The time derivative of the PDF along the trajectory of (32) is

$$\begin{aligned} \dot{V} &= \gamma_e \dot{e}_p^T \ddot{e}_p + \gamma_e \omega_0^2 \dot{e}_p^T e_p \\ &+ \text{tr} \left\{ \gamma_R^{-1} \tilde{R} \dot{\tilde{R}}^T + \gamma_D^{-1} \tilde{D} \dot{\tilde{D}}^T + \gamma_\Omega^{-1} \tilde{\Omega} \dot{\tilde{\Omega}}^T \right\} \\ &= \gamma_e \dot{e}_p^T \tau_1 + \gamma_e \dot{e}_p^T \tilde{u} \\ &+ \text{tr} \left\{ \gamma_R^{-1} \tilde{R} \dot{\tilde{R}}^T + \gamma_D^{-1} \tilde{D} \dot{\tilde{D}}^T + \gamma_\Omega^{-1} \tilde{\Omega} \dot{\tilde{\Omega}}^T \right\}. \end{aligned} \quad (34)$$

If τ_1 is chosen to be

$$\tau_1 = -\gamma_e \dot{e}_p \quad (35)$$

then (34) becomes

$$\begin{aligned} \dot{V} &= -\gamma_e^2 \dot{e}_p^T \dot{e}_p + \text{tr} \left\{ \tilde{R} \left(\gamma_R^{-1} \dot{\tilde{R}}^T - \frac{1}{2} \dot{q} \tau_1^T - \frac{1}{2} \tau_1 \dot{q}^T \right) \right\} \\ &+ \text{tr} \left\{ \tilde{D} \left(\gamma_D^{-1} \dot{\tilde{D}}^T - \frac{1}{2} \dot{q} \tau_1^T - \frac{1}{2} \tau_1 \dot{q}^T \right) \right\} \\ &+ \text{tr} \left\{ \tilde{\Omega} \left(\gamma_\Omega^{-1} \dot{\tilde{\Omega}}^T - \dot{q} \tau_1^T + \tau_1 \dot{q}^T \right) \right\}. \end{aligned} \quad (36)$$

Therefore, the parameter adaptation laws

$$\begin{aligned} \dot{\tilde{R}} &= \frac{1}{2} \gamma_R (\tau_1 \dot{q}^T + \dot{q} \tau_1^T) \\ \dot{\tilde{D}} &= \frac{1}{2} \gamma_D (\tau_1 \dot{q}^T + \dot{q} \tau_1^T) \\ \dot{\tilde{\Omega}} &= \gamma_\Omega (\tau_1 \dot{q}^T - \dot{q} \tau_1^T) \end{aligned} \quad (37)$$

lead to $\dot{V} = -\gamma_e^2 \dot{e}_p^T \dot{e}_p \leq 0$.

Theorem 3: With the control laws (31) and (35) and the parameter adaptation laws (37), the total energy error $\tilde{E} = 1/2(\dot{q}^T \dot{q} + \omega_0^2 q^T q) - E_0$, the angular momentum, and their time derivatives converge to zero.

Proof: $\dot{V} \leq 0$ implies that $V(t) \leq V(0)$. Thus, V is bounded. The derivative of \dot{V} is

$$\begin{aligned} \ddot{V} &= -2\gamma_e^2 \dot{e}_p^T \ddot{e}_p \\ &= -2\gamma_e^2 \dot{e}_p^T (-\omega_0^2 e_p + \tau_1 + \tilde{u}). \end{aligned}$$

This shows that \ddot{V} is also bounded. Therefore, by Barbalat's lemma, $\dot{V} \rightarrow 0$, or, equivalently, $\dot{e}_p \rightarrow 0$. Taking one more derivative of the trajectory error equation gives

$$\begin{aligned} \ddot{e}_p &= -\omega_0^2 \dot{e}_p - \gamma_e \ddot{e}_p + \dot{\tilde{u}} \\ &= -\omega_0^2 \dot{e}_p - \gamma_e (-\omega_0^2 e_p - \gamma_e \dot{e}_p + \tilde{u}) + \dot{\tilde{u}}. \end{aligned}$$

Thus, \ddot{e}_p is also bounded. Application of the Barbalat's lemma indicates that $\ddot{e}_p \rightarrow 0$, implying that $e_p \rightarrow \tilde{u}$. On the other hand, the integral error equation gives

$$\begin{aligned} \omega_0^2 \int_0^\infty e_p dt &= \int_0^\infty (-\ddot{e}_p - \gamma_e \dot{e}_p + \tilde{u}) dt \\ &= -\dot{e}_p|_0^\infty - \gamma_e e_p|_0^\infty + \int_0^\infty \tilde{u} dt. \end{aligned}$$

Thus, the integral of e_p is bounded. Again, by Barbalat's lemma, $e_p \rightarrow 0$, and $\tilde{u} \rightarrow 0$. Since, as $t \rightarrow \infty$ trajectory of the nonideal gyroscope follows that of the ideal gyroscope, $\tilde{E} \rightarrow 0$, $\dot{\tilde{E}} \rightarrow 0$, $P \rightarrow 0$, and $\dot{P} \rightarrow 0$ are achieved. ■

Therefore, with this control scheme, the trajectory of the gyroscope can be controlled while preserving all convergence properties of the adaptive control discussed in Section IV.

B. Convergence-Rate Analysis

As Theorem 1 indicates, if the trajectory is forced to converge to an oscillatory motion along the x -axis, the drive-axis frequency, the quadrature, and the angular rate with cross-damping term are estimated and compensated for. In this section, the convergence rate of these parameters is derived.

Averaging analysis is commonly used in the adaptive control literature [8] and will be used to estimate the convergence properties of the gyroscope parameter estimates. The convergence rate of the angular-rate estimate is important because it determines the bandwidth of the gyroscope. By using the fact that the parameter estimation dynamics is slower than the trajectory dynamics, we can relate the slow parameter estimation dynamics with the averaged parameter estimation dynamics. By using the fact that the products of sinusoids at different frequencies have zero average, the averaged dynamics of the parameter error estimates can be obtained as follows:

$$\begin{aligned} \dot{\omega}_x|_{\text{avg}} &\approx -\frac{\gamma_R}{2} X_0^2 \omega_x^2|_{\text{avg}} \\ \dot{\omega}_{xy}|_{\text{avg}} &\approx -\frac{\gamma_R}{4} X_0^2 \omega_{xy}|_{\text{avg}} \\ \dot{d}_{xx}|_{\text{avg}} &\approx -\frac{\gamma_D}{2} X_0^2 \omega_0^2 d_{xx}|_{\text{avg}} \\ (\dot{d}_{xy} + 2\dot{\Omega}_z)|_{\text{avg}} &\approx -\frac{1}{4}(\gamma_D + 4\gamma_\Omega) X_0^2 \omega_0^2 (\tilde{d}_{xy} + 2\tilde{\Omega}_z)|_{\text{avg}}. \end{aligned} \quad (38)$$

By assuming that $\tilde{d}_{xy} = 0$, the average dynamics of the angular-rate estimate is approximately given by

$$\dot{\tilde{\Omega}}_z|_{\text{avg}} \approx -\gamma_\Omega X_0^2 \omega_0^2 \tilde{\Omega}_z|_{\text{avg}} \quad (39)$$

and the bandwidth of the adaptive controlled gyroscope is approximately given by $\text{BW} \approx \gamma_\Omega X_0^2 \omega_0^2$. Thus, the bandwidth of a MEMS gyroscope under adaptive control is proportional to the adaptation gain and the energy of oscillation of the reference model.

C. Modification of Adaptation Laws

Theorem 2 indicates that if the condition (26) is satisfied while the trajectory is switched from the oscillation along \hat{v}_1 to the oscillation along $\hat{v}_2 \neq \hat{v}_1$, then $\tilde{R} \rightarrow 0$, $\tilde{D} \rightarrow 0$, and $\tilde{\Omega} \rightarrow 0$ are guaranteed. This condition can be satisfied by introducing the following modification to the adaptation laws (37).

By considering (36), the idea behind the selection of the adaptation laws is to make the terms that contain parameter adaptation errors equal to zero, i.e.,

$$\begin{aligned} &\text{tr} \left\{ \tilde{R} \left(\gamma_R^{-1} \dot{\tilde{R}}^T - \frac{1}{2} q \tau_1^T - \frac{1}{2} \tau_1 q^T \right) \right\} \\ &+ \text{tr} \left\{ \tilde{D} \left(\gamma_D^{-1} \dot{\tilde{D}}^T - \frac{1}{2} \dot{q} \tau_1^T - \frac{1}{2} \tau_1 \dot{q}^T \right) \right\} \\ &+ \text{tr} \left\{ \tilde{\Omega} \left(\gamma_\Omega^{-1} \dot{\tilde{\Omega}}^T - \dot{q} \tau_1^T + \tau_1 \dot{q}^T \right) \right\} = 0. \end{aligned} \quad (40)$$

The modification in the adaptation laws should preserve (40) and should also satisfy the convergence properties of (26). By rearranging (40), we obtain

$$\begin{aligned} &\text{tr} \left\{ 2\gamma_R^{-1} \tilde{R} \dot{\tilde{R}}^T + 2\gamma_D^{-1} \tilde{D} \dot{\tilde{D}}^T + 2\gamma_\Omega^{-1} \tilde{\Omega} \dot{\tilde{\Omega}}^T \right\} \\ &- \text{tr} \left\{ \tau_1^T \tilde{R} q + q^T \tilde{R} \tau_1 + \tau_1^T (\tilde{D} + 2\tilde{\Omega}) \dot{q} + \dot{q}^T (\tilde{D} - 2\tilde{\Omega}) \tau_1 \right\} = 0. \end{aligned} \quad (41)$$

To satisfy the convergence properties in (26), it is useful to decompose q , \dot{q} , and τ_1 into their parallel and normal components with respect to the unit vector \hat{v}_1

$$\begin{aligned} q &= q_n + q_p \\ \dot{q} &= \dot{q}_n + \dot{q}_p \\ \tau_1 &= \tau_{1n} + \tau_{1p} \end{aligned} \quad (42)$$

where subscripts n and p stand for normal and parallel components to \hat{v}_1 . Substituting (42) into (41) yields

$$\begin{aligned} &\text{tr} \left\{ 2\gamma_R^{-1} \tilde{R} \dot{\tilde{R}}^T + 2\gamma_D^{-1} \tilde{D} \dot{\tilde{D}}^T + 2\gamma_\Omega^{-1} \tilde{\Omega} \dot{\tilde{\Omega}}^T \right\} \\ &- \text{tr} \left\{ (\tau_{1n} + \tau_{1p})^T \tilde{R} (q_n + q_p) + (q_n + q_p)^T \tilde{R} (\tau_{1n} + \tau_{1p}) \right\} \\ &- \text{tr} \left\{ (\tau_{1n} + \tau_{1p})^T (\tilde{D} + 2\tilde{\Omega}) (\dot{q}_n + \dot{q}_p) \right. \\ &\quad \left. + (\dot{q}_n + \dot{q}_p)^T (\tilde{D} - 2\tilde{\Omega}) (\tau_{1n} + \tau_{1p}) \right\} = 0. \end{aligned} \quad (43)$$

Convergence properties (26) simplify (43) further

$$\begin{aligned} &\text{tr} \left\{ 2\gamma_R^{-1} \tilde{R} \dot{\tilde{R}}^T + 2\gamma_D^{-1} \tilde{D} \dot{\tilde{D}}^T + 2\gamma_\Omega^{-1} \tilde{\Omega} \dot{\tilde{\Omega}}^T \right\} \\ &- \text{tr} \left\{ \tau_{1n}^T \tilde{R} q_n + q_n^T \tilde{R} \tau_{1n} \right\} \\ &- \text{tr} \left\{ \tau_{1n}^T \tilde{D} \dot{q}_n + \dot{q}_n^T \tilde{D} \tau_{1n} + \tau_{1p}^T (\tilde{D} + 2\tilde{\Omega}) \dot{q}_n \right. \\ &\quad \left. + \dot{q}_n^T (\tilde{D} - 2\tilde{\Omega}) \tau_{1p} \right\} = 0. \end{aligned} \quad (44)$$

TABLE I
 KEY PARAMETERS OF THE GYROSCOPE

parameter	value
mass	$5.095 \times 10^{-7} kg$
x -axis frequency	4.17 KHz
Quality factor	40
Brownian noise PSD	$5.53 \times 10^{-24} N^2 sec$
Ideal velocity noise PSD	$1.02 \times 10^{-18} (m/sec)^2 sec$

Finally, we have

$$\begin{aligned}
 & \text{tr} \left\{ \tilde{R} \left(\gamma_R^{-1} \dot{\tilde{R}}^T - \frac{1}{2} q_n \tau_{1n}^T - \frac{1}{2} \tau_{1n} q_n^T \right) \right\} \\
 & + \text{tr} \left\{ \tilde{D} \left(\gamma_D^{-1} \dot{\tilde{D}}^T - \frac{1}{2} \dot{q}_n \tau_{1n}^T - \frac{1}{2} \tau_{1n} \dot{q}_n^T \right) \right\} \\
 & + \text{tr} \left\{ \tilde{\Omega} \left(\gamma_\Omega^{-1} \dot{\tilde{\Omega}}^T - \dot{q}_n \tau_{1p}^T + \tau_{1p} \dot{q}_n^T \right) \right\} = 0. \quad (45)
 \end{aligned}$$

Therefore, the modified adaptation laws that satisfy the conditions in Theorem 2 are given as follows:

$$\begin{aligned}
 \dot{\tilde{R}} &= \frac{1}{2} \gamma_R (\tau_{1n} q_n^T + q_n \tau_{1n}^T) \\
 \dot{\tilde{D}} &= \frac{1}{2} \gamma_D (\tau_{1n} \dot{q}_n^T + \dot{q}_n \tau_{1n}^T) \\
 \dot{\tilde{\Omega}} &= \gamma_\Omega (\tau_{1p} \dot{q}_n^T - \dot{q}_n \tau_{1p}^T) \quad (46)
 \end{aligned}$$

where $\gamma_D/2 = 2\gamma_\Omega$. These adaptation laws are used in place of (37) while the trajectory switches.

Although the online identification and compensation of all major fabrication imperfections and their variations are highly desirable to achieve robust and high-performance gyroscope operation, the proposed trajectory-switching algorithm is not suitable to the online operation because continuous switching must be involved during the gyroscope operation. Instead, the switching algorithm can be used at the initial calibration stage when the gyroscope is turned on or at regular calibration sessions which may periodically be performed to identify fabrication imperfections. Once imperfections are identified, their values can be frozen until the next calibration session and be used for the adaptive force-balancing control without the trajectory-switching algorithm because the variation of the fabrication imperfections is negligibly slow compared with that of the angular rate.

VI. SIMULATIONS

A simulation study using the preliminary design data of the Massachusetts Institute of Technology-Silicon on Insulator (MIT-SOI) MEMS gyroscope was conducted to evaluate the proposed algorithm. The data of some of the gyroscope parameters in the model are summarized in Table I. For simulation purposes, we allowed $\pm 20\%$ parameter variations for the spring and damping coefficients and assumed $\pm 10\%$ magnitude of

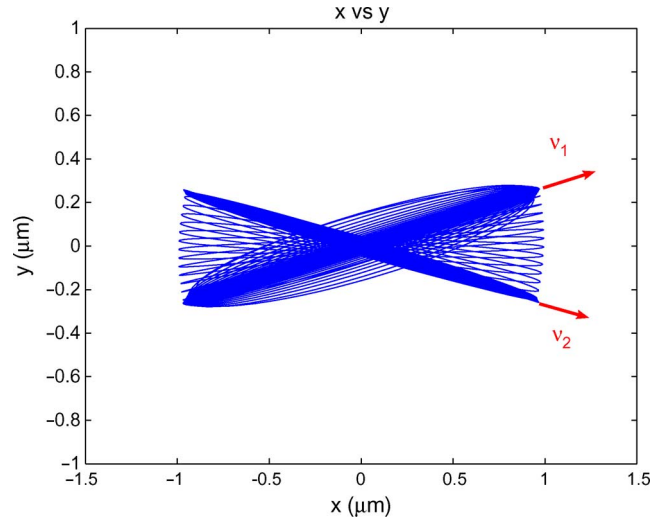


Fig. 2. Trajectory of the proof mass in the x - y plane.

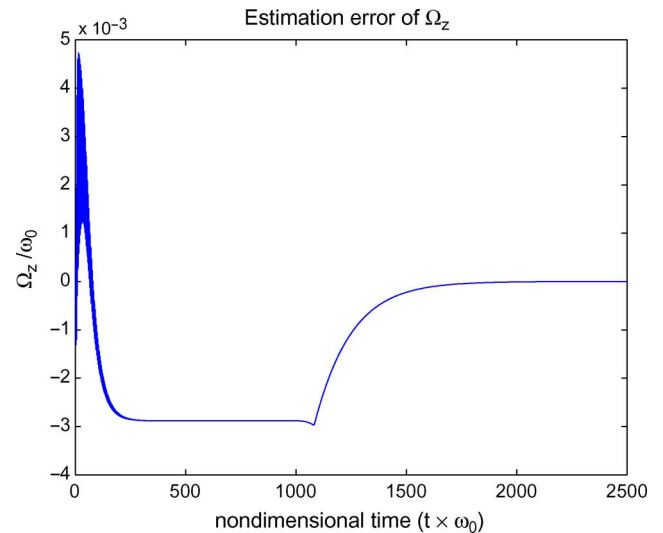


Fig. 3. Time response of the angular-rate estimate error.

nominal spring and $\pm 0.1\%$ magnitude of nominal damping coefficients for their off-diagonal terms. Note that the simulation results are shown in nondimensional units, which are nondimensionalized based on the proof mass, the length of $1 \mu m$, and the x -axis nominal natural frequency.

Fig. 2 shows the trajectories of the proof mass of the gyroscope in the x - y plane. With the control laws (31) and (35) and the parameter adaptation laws (46), the trajectory of the proof mass has first converged to a straight line of the slope angle $+15^\circ$ (\hat{v}_1 direction in Fig. 2). After switching occurs at $t = 1000$ nondimensional time, the trajectory converges to a straight line of the slope angle -15° (\hat{v}_2 direction in Fig. 2). Figs. 3–5 show the simulation results which illustrate the convergence properties of the trajectory-switching adaptive control scheme designed in this paper. Note that before the trajectory is switched, all parameter estimates are biased, but after the trajectory switching occurs, all parameter estimates converge to their true values. Figs. 6 and 7 show the estimate of angular-rate response to the step and the sinusoidal input angular rates after freezing the estimated parameters obtained by switching.

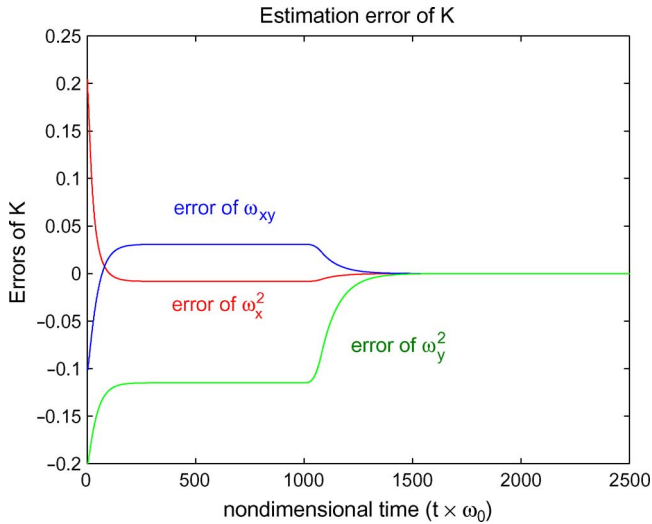


Fig. 4. Time responses of the frequency estimate errors.

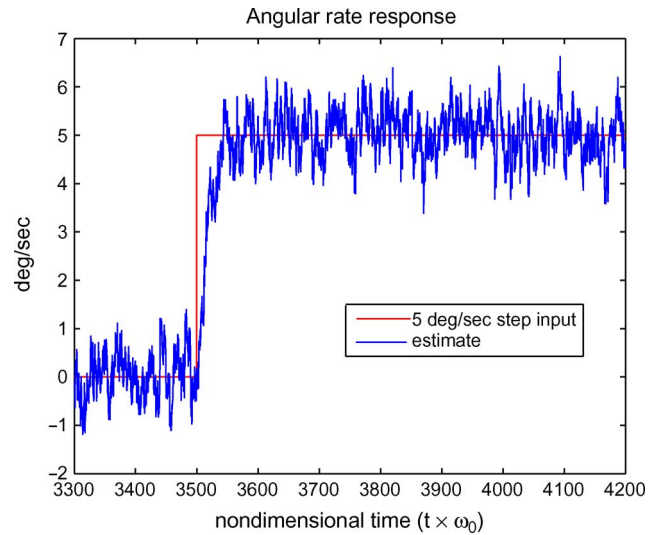


Fig. 6. Time response of the angular-rate estimate to the 5^{deg/s} step input.

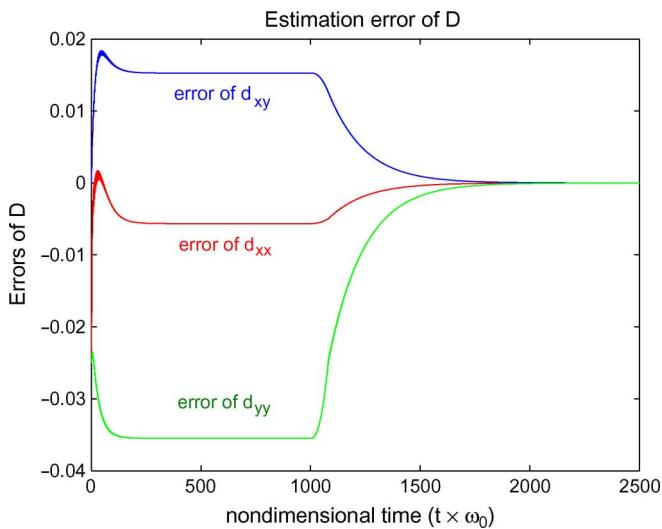


Fig. 5. Time responses of the damping estimate errors.

The simulation supports the convergence results derived for the trajectory-switching adaptive control scheme.

VII. CONCLUSION

Dynamic analysis of typical MEMS gyroscopes shows that fabrication imperfections are a major factor limiting the performance of the gyroscope. However, the conventional force-balancing-controlled gyroscope in a mode-matched operation does not have sufficient persistence of excitation and as a result, all major fabrication imperfections cannot be identified and compensated for.

This paper proposed the adaptive force-balancing control with a trajectory-switching algorithm. By switching the trajectory of the proof mass of a gyroscope, additional richness of excitation is supplied to the internal dynamics of the gyroscope, and thus, the quadrature compensation, the drive- and sense-axis frequency tuning, and the closed-loop identification of the angular rate are possible. The proposed control scheme does not rely on the measurement of the input/output phase difference

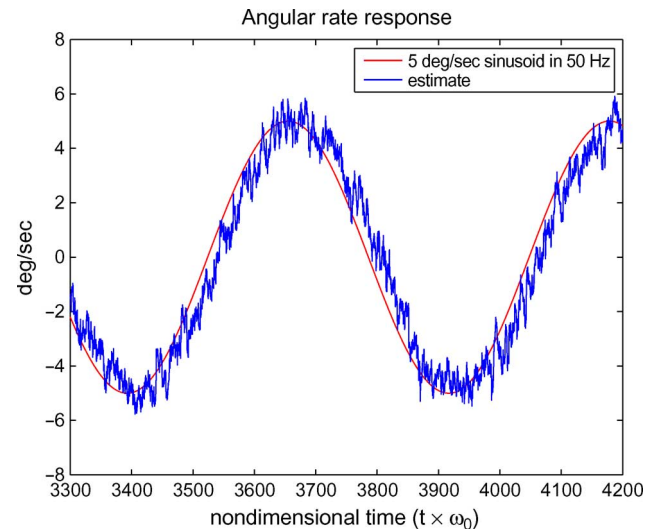


Fig. 7. Time response of the angular-rate estimate to the 5^{deg/s} sinusoid input at 50 Hz.

and does not produce ZRO, which is caused by the cross-damping terms.

A simulation study using the preliminary design data of the MIT-SOI MEMS gyroscope was conducted to evaluate the proposed control scheme. Simulation results supported the convergence results derived for the trajectory-switching adaptive control scheme.

REFERENCES

- [1] N. Yazdi, F. Ayazi, and K. Najafi, "Micromachined inertial sensors," *Proc. IEEE*, vol. 86, no. 8, pp. 1640–1659, Aug. 1998.
- [2] A. Shkel, R. T. Howe, and R. Horowitz, "Modeling and simulation of micromachined gyroscopes in the presence of imperfection," in *Proc. Int. Conf. Modelling Simul. Microsyst.*, San Juan, PR, 1999, pp. 605–608.
- [3] S. Park and R. Horowitz, "Adaptive control for the conventional mode of operation of MEMS gyroscope," *J. Microelectromech. Syst.*, vol. 12, no. 1, pp. 101–108, Feb. 2003.
- [4] X. Jiang, J. Seeger, M. Kraft, and B. E. Boser, "A monolithic surface micromachined Z-axis gyroscope with digital output," in *Proc. IEEE Symp. VLSI Circuits*, Honolulu, HI, Jun. 2000, pp. 16–19.

- [5] S. Chang, M. Chia, P. Castillo-Borelley, W. Higdon, Q. Jiang, J. Johnson, L. Obedier, M. Putty, Q. Shi, D. Sparks, and S. Zarabadi, "An electroformed CMOS integrated angular rate sensor," *Sens. Actuators A, Phys.*, vol. 66, no. 1–3, pp. 138–143, Apr. 1998.
- [6] A. M. Shkel, R. Horowitz, A. A. Seshia, S. Park, and R. T. Howe, "Dynamics and control of micromachined gyroscopes," in *Proc. IEEE Amer. Control Conf.*, Jun. 1999, pp. 2119–2124.
- [7] J. Slotine and W. Li, *Applied Nonlinear Control*. Englewood Cliffs, NJ: Prentice-Hall, 1991.
- [8] S. S. Sastry, *Adaptive Control: Stability, Convergence and Robustness*. Englewood Cliffs, NJ: Prentice-Hall, 1989.
- [9] W. A. Clark, "Micromachined vibratory rate gyroscopes," Ph.D. dissertation, Univ. California, Berkeley, Berkeley, CA, 1997.



Sungsu Park received the B.S. and M.S. degrees in aerospace engineering from Seoul National University, Seoul, Korea, in 1988 and 1990, respectively, and the Ph.D. degree in mechanical engineering from the University of California at Berkeley in 2000.

He is currently an Associate Professor with the Department of Aerospace Engineering, Sejong University, Seoul. His research interests include estimation theory, adaptive and robust control with applications to microelectromechanical systems, and aerospace systems.



Roberto Horowitz (M'82) was born in Caracas, Venezuela, in 1955. He received the B.Sc. degree in mechanical engineering (with highest honors) and the Ph.D. degree from the University of California at Berkeley in 1978 and 1983, respectively.

Since 1982, he has been with the Department of Mechanical Engineering, University of California at Berkeley, where he is currently a Professor. He teaches and conducts research in the areas of adaptive, learning, nonlinear, and optimal control with applications to microelectromechanical systems, mechatronics, robotics, and intelligent vehicle and highway systems.

Dr. Horowitz is a member of the American Society of Mechanical Engineers. He was the recipient of the 1984 IBM Young Faculty Development Award and the 1987 NSF Presidential Young Investigator Award.



Sung Kyung Hong received the B.S. and M.S. degrees from Yonsei University, Seoul, Korea, in 1987 and 1989, respectively, and the Ph.D. degree in mechanical engineering from Texas A&M University, College Station, in 1998.

From 1989 to 2000, he was with the Unmanned Aerial Vehicle (UAV) System Division and Flight Dynamics and Control Laboratory, Agency for Defense Development, Korea. He is currently an Associate Professor with the Department of Aerospace Engineering, Sejong University, Seoul. His research

interests include fuzzy logic controls, inertial sensor applications, and flight control systems for UAVs.



Yoonsu Nam received the B.S. degree in nuclear engineering and the M.S. degree in mechanical engineering from Seoul National University, Seoul, Korea, in 1981 and 1983, respectively, and the Ph.D. degree in mechanical engineering from the Georgia Institute of Technology, Atlanta, in 1991, where he worked on the tip position control of a flexible manipulator using a proof mass.

From 1992 to 1996, he was with the Flight Dynamics and Control Laboratory, Agency for Defense Development, Korea. He is currently a Professor with the Department of Mechanical and Mechatronics Engineering, Kangwon National University, Chuncheon, Korea. His main research interests are control theory and its applications.